MDPI

*Article*

# TRIDENT-DE: Triple-Operator Differential Evolution with Adaptive Restarts and Greedy Refinement

**Vasileios Charilogis[1], Ioannis G. Tsoulos[2,*] and Gianni Anna Maria[3]**

[1] Department of Informatics and Telecommunications, University of Ioannina, 47150 Kostaki Artas, Greece, v.charilog@uoi.gr
[2] Department of Informatics and Telecommunications, University of Ioannina, 47150 Kostaki Artas, Greece, itsoulos@uoi.gr
[3] Department of Informatics and Telecommunications, University of Ioannina, 47150 Kostaki Artas, Greece, am.gianni@uoi.gr
* Correspondence: itsoulos@uoi.gr

**Abstract:** This paper introduces TRIDENT-DE, a novel ensemble-based variant of Differential Evolution (DE) designed to tackle complex continuous global optimization problems. The algorithm leverages three complementary trial vector generation strategies best/1/bin, current-to-best/1/bin, and pbest/1/bin executed within a self-adaptive framework that employs jDE parameter control. To prevent stagnation and premature convergence, TRIDENT-DE incorporates adaptive micro-restart mechanisms, which periodically reinitialize a fraction of the population around the elite solution using Gaussian perturbations, thereby sustaining exploration even in rugged landscapes. Additionally, the algorithm integrates a greedy line-refinement operator that accelerates convergence by projecting candidate solutions along promising base-to-trial directions. These mechanisms are coordinated within a mini-batch update scheme, enabling aggressive iteration cycles while preserving diversity in the population. Experimental results across a diverse set of benchmark problems, including molecular potential energy surfaces and engineering design tasks, show that TRIDENT-DE consistently outperforms or matches state-of-the-art optimizers in terms of both best-found and mean performance. The findings highlight the potential of multi-operator, restart-aware DE frameworks as a powerful approach to advancing the state of the art in global optimization.

**Keywords:** Differential evolution, Metaheuristics, Regenerative Computing, Hybridization, Evolutionary Algorithms, Global Optimization, Mutation Strategies,

**Citation:** Charilogis, V., Tsoulos, I.G., Gianni, A. M.. TRIDENT-DE: Triple-Operator Differential Evolution with Adaptive Restarts and Greedy Refinement. *Journal Not Specified* **2024**, *1*, 0.

Received:
Revised:
Accepted:
Published:



## 1. Introduction

Global optimization remains a central challenge in computational science, offering indispensable tools for addressing problems of high complexity in diverse domains ranging from engineering and physics to economics, biology, and artificial intelligence. Unlike local search methods that tend to converge toward nearby minima and thus risk entrapment in suboptimal solutions, global optimization seeks to explore the search space more comprehensively in order to identify the true global optimum. The inherent difficulty of such tasks arises from the presence of multimodality, discontinuities, nonconvex structures, and high dimensionality, all of which demand algorithmic strategies that balance exploration with exploitation in a highly adaptive manner.

Global optimization is most clearly grounded in its mathematical formulation. Let $f : S \to \mathbb{R}$ be a continuous real-valued function defined on a feasible region $S \subset \mathbb{R}^n$. The goal is to determine a global minimizer $x^\star \in S$ such that $f(x^\star) \leq f(x)$ for all $x \in S$. The feasible region is typically modeled as a Cartesian product of closed and bounded intervals, $S = \prod_{i=1}^{n} [a_i, b_i]$, ensuring that $S$ is compact (and convex under interval bounds). Under these conditions, optimization becomes the systematic pursuit of the minimizer within a well-defined, yet potentially rugged and high-dimensional, landscape.

Over the past decades, a wide variety of optimization algorithms have been introduced, evolving from traditional deterministic approaches to powerful modern metaheuristics. Classical derivative-based methods, such as steepest descent [1] and Newton's method [2], are efficient for smooth and convex problems but struggle in the absence of gradient information or in the presence of multiple minima. Stochastic search methods like Monte Carlo sampling [3] and simulated annealing [4] introduced robustness to noise and multimodality but at the expense of slower convergence.

A particularly influential family of methods has been population-based metaheuristics. Genetic Algorithms (GA) [5], Differential Evolution (DE) [6–9], and Particle Swarm Optimization (PSO) [10–12] remain standard references in this field, each exploiting collective dynamics of populations to efficiently explore the solution space. Within this lineage, numerous refinements have been proposed to enhance adaptivity and performance. Self-adaptive Differential Evolution (SaDE) [13] and jDE [14] introduced mechanisms whereby control parameters co-evolve alongside candidate solutions, leading to more resilient search dynamics. Comprehensive Learning Particle Swarm Optimization (CLPSO) [15] extended the PSO paradigm by enhancing the information-sharing process across the swarm, thus improving the ability to escape local minima. The Covariance Matrix Adaptation Evolution Strategy (CMA-ES) [16], often regarded as one of the most sophisticated evolutionary optimizers, dynamically adapts covariance structures to guide search more effectively in anisotropic landscapes.

Recent years have also seen the development of highly specialized and hybrid approaches that push the limits of global optimization. The EA4Eig algorithm [17] exploits eigenspectrum information to adjust search directions more intelligently. The UDE3 (also known as UDE-III) method [18] introduces novel recombination schemes that maintain diversity while emphasizing convergence. The mLSHADE_RL variant [19] integrates reinforcement learning into the LSHADE family to adapt parameter settings more effectively across evolving search states. Such developments underscore a continuing trend toward hybridization and adaptivity, in which classical frameworks are enriched by dynamic control, learning mechanisms, or hybrid ensembles of operators.

Derivative-free approaches such as the Nelder-Mead simplex [20] retain relevance in low-dimensional and gradient-free scenarios, while biologically and physically inspired heuristics such as ant colony optimization [21] and artificial bee colony [22] continue to provide innovative perspectives by mimicking natural processes. These diverse algorithmic families collectively form the backbone of contemporary global optimization research, where robustness, scalability, and adaptivity remain the primary objectives.

The present article introduces TRIDENT-DE, a novel algorithmic framework that distinguishes itself from the aforementioned methodologies through its explicit reliance on a triple-operator ensemble structure combined with adaptive restart and greedy refinement strategies. Unlike standard Differential Evolution variants that typically rely on a single trial vector generation scheme, TRIDENT-DE simultaneously employs best/1/bin, current-to-best/1/bin, and pbest/1/bin within a self-adaptive mechanism, ensuring a dynamic balance between exploration and exploitation. This triadic structure, metaphorically represented as a "trident," allows the algorithm to probe the search space from complementary perspectives, thereby reducing the likelihood of premature convergence. Furthermore, TRIDENT-DE incorporates a micro-restart mechanism that reinitializes a fraction of the population around the elite solution with Gaussian perturbations, preserving diversity without discarding accumulated information. An additional greedy line-refinement operator accelerates convergence by projecting solutions along base-to-trial directions, enabling more aggressive exploitation of promising regions. In contrast to hybrid algorithms that often combine unrelated strategies in ad hoc ways, TRIDENT-DE presents a cohesive framework where each component synergistically reinforces the others, yielding a method that is not only adaptive and robust but also computationally efficient. This conceptual and practical novelty positions TRIDENT-DE as a competitive advancement in the landscape of

global optimization, capable of addressing high-dimensional, multimodal problems with a level of aggressiveness and resilience that surpasses existing methods.

The remainder of this paper is organized as follows: Section 2 details TRIDENT-DE, including design rationale and implementation aspects. Section 3 introduces the experimental protocol and results: Subsection 3.1 summarizes settings and computational environment, Subsection 3.2 enumerates the benchmark suites with emphasis on real-world instances, Subsection 3.3 analyzes parameter sensitivity, Subsection 3.4 examines time complexity and scaling behavior, and Subsection 3.5 reports the comparative assessment against state-of-the-art solvers. Finally, Section 4 concludes with key findings and directions for future work.

## 2. The TRIDENT-DE method

We now present the pseudocode of TRIDENT-DE to make the full control loop explicit. Before diving into it, recall that updates are executed in mini-batches: each agent builds multiple trials using three complementary Differential Evolution operators and retains the best one. A low-cost greedy line refinement is then applied along the base-to-trial direction, while parameters are perturbed via light self-adaptation. Iteration-level progress is assessed explicitly, when stagnation is detected, adaptive micro-restarts refresh diversity without disrupting exploitation around the elite. Feasibility is enforced by box projection, and termination follows an evaluation budget or a maximum-iteration cap. With this context, the pseudocode below summarizes the stages and decision points implemented in TRIDENT-DE.

**Algorithm 1** TRIDENT-DE (Triple-Operator, Restart-Aware DE)

Input: objective $f$, dimension $n$, population $N$, max iters $I_{max}$, max evals $FE_{max}$, bounds $\ell, u$

Params: base $F$, crossover $C$, operator probs $r, q, p$ (best/1, cur2best/1, pbest/1), stagnation trigger $\tau$, restart fraction $\rho$, elite size $\kappa$, jitter amplitude $\lambda$, elite-kick prob $\pi$, line-refine factor $\beta$

**01 For** i = 1..$N$ **do**
**02** **For** j = 1..$n$ **do**
03 sample $x_{i,j}$ from Uniform($\ell_j, u_j$)
**04** **End for**
05 $y_i \leftarrow f(x_i)$
06 **End for**
07 $i^\star \leftarrow \arg\min_i y_i$ , $x^\star \leftarrow x_{i^\star}$ , $f^\star \leftarrow y_{i^\star}$ , $A \leftarrow \{x^\star\}$ $t \leftarrow 0$, FE $\leftarrow N$, $s \leftarrow 0$
08 **While** $(t < I_{max})$ and $(FE < FE_{max})$ **do**
09 $t \leftarrow t + 1$ , update $i^\star, x^\star, f^\star$
10 **For** $i$ = 1..$N$ **do**
11 **If** i = $i^*$ **then** continue
12 $x^0 \leftarrow x_i$, $f^0 \leftarrow y_i$
13 Draw op from {best/1 with prob $r$, cur2best/1 with prob $q$, pbest/1 with prob $p$, none with prob $1 - (r + q + p)$}
14 $F \leftarrow \text{clip}(F + \lambda\,\mathcal{N}(0,1), 0, 2)$, $C_i \leftarrow \text{clip}(C + \lambda\,\mathcal{N}(0,1), 0, 1)$
15 $r_1 \neq i, r_2 \neq i, r_2 \neq r_1$
16 **If** op = best/1 then $v \leftarrow x^\star + F_i(x_{r_1} - x_{r_2})$
17 **Else if** op = cur2best/1 **then** $v \leftarrow x_i + F_i \cdot (x^\star - x_i) + F_i \cdot (x_{r_1} - x_{r_2})$
18 **Else if** op = pbest/1 **then** pick $p^\star \in A \cup x^\star$ , $v \leftarrow p^\star + F_i \cdot (x_{r_1} - x_{r_2})$
19 **Else** $v \leftarrow x_i$
20 **End if**
21 Pick $j_{rand}$ uniformly from {1..$n$}
22 **For** $j$ = 1..$n$ **do**
23 **If** Uniform(0,1) < $C_i$ **or** $j = j_{rand}$ **then** $z_j \leftarrow v_j$ **else** $z_j \leftarrow x_{i,j}$
24 $z_j \leftarrow clamp(z_j, \ell_j, u_j)$
25 **End for**
26 $g \leftarrow z - x_i$ , $x^\top \leftarrow clamp(x_i + \beta \cdot g, \ell, u)$ , $f^\top \leftarrow f(x^\top)$ , $FE \leftarrow FE + 1$
27 **If** $f^\top < f^0$ **then**
28 $x_i \leftarrow x^\top$, $y_i \leftarrow f^\top$
29 **If** $y_i < f^*$ **then** $x^* \leftarrow x_i$, $f^\star \leftarrow y_i$, $s \leftarrow 0$, update elite ring $A$ keeping $|A| \leq \kappa$
30 **Else** $f^z \leftarrow f(z)$, $FE \leftarrow FE + 1$
31 **If** $f^z < f^0$ **then**
32 $x_i \leftarrow z$,$y_i \leftarrow f^z$
33 **If** $y_i < f^*$ then $x^\star \leftarrow x_i$, $f^\star \leftarrow y_i$, $s \leftarrow 0$
37 **Else** $x_i \leftarrow x^0$, $y_i \leftarrow f^0$
39 **End if**
40 **End if**
41 **End for**
42 **If** no $y_i$ improved **then** $s \leftarrow s + 1$ **else** $s \leftarrow 0$
43 **If** $s \geq \tau$ **then**
44 $m \leftarrow \lfloor \rho \cdot N \rfloor$, pick worst $m$ indices set $W$
45 **For** each i in $W$ **do**
46 **If** Uniform(0,1) < $\pi$ **then** sample $x_i$ from $\mathcal{N}(x, \sigma^2 \cdot (u - \ell)^2)$ else sample each $x_{i,j}$ from Uniform($\ell_j, u_j$)
47 Project $x_i$ to box $[\ell, u]$, $y_i \leftarrow f(x_i)$, $FE \leftarrow FE + 1$
48 **End for**
49 $s \leftarrow 0$
50 **End if**
51 **End while**
52 **Return** $x^\star$, $f^\star$

Notes for pseudocode.

*Objective and domain.* $f : S \to \mathbb{R}$, $S = [\ell, u] = \prod_{j=1}^{n} [\ell_j, u_j]$. *A candidate is* $x \in \mathbb{R}^n$.
*Population and elite. Size* $N$, $x_i$ *is the i-th individual,* $y_i = f(x_i)$. *Best index* $i^\star = \arg\min_i y_i$, *elite* $x^\star = x_{i^\star}$, $f^\star = f(x^\star)$. *Elite archive* $A$ *holds up to* $\kappa$ *best solutions (ties by* $f$*).*
*Operators. One of* ***best/1***, ***current-to-best/1***, ***pbest/1***, *or* ***none***, *drawn with probabilities* $(r, q, p, 1-(r+q+p))$. *With* $r_1 \neq r_2 \neq i$*:*

$$\begin{aligned} \textbf{\textit{best/1:}}\ & v = x^\star + F_i(x_{r_1} - x_{r_2}), \\ \textbf{\textit{current-to-best/1:}}\ & v = x_i + F_i(x^\star - x_i) + F_i(x_{r_1} - x_{r_2}), \\ \textbf{\textit{pbest/1:}}\ & p^\star \sim \mathrm{Unif}(A \cup \{x^\star\}),\ v = p^\star + F_i(x_{r_1} - x_{r_2}), \\ \textbf{\textit{none:}}\ & v = x_i. \end{aligned}$$

*Controls. Per-individual jitter* $F_i = \mathrm{clip}(F + \lambda_F \xi_F, 0, 2)$ *and* $C_i = \mathrm{clip}(C + \lambda_C \xi_C, 0, 1)$ *with* $\xi_F, \xi_C \sim \mathcal{N}(0,1)$. *Scalar* $\mathrm{clip}(x, a, b) = \min\{\max\{x, a\}, b\}$*; vector* $\mathrm{clamp}(x, \ell, u)$ *applies* clip *component-wise.*
*Crossover and projection. Binomial crossover with rate* $C_i$ *and one forced index* $j_{\mathrm{rand}}$ *from* $v$ *ensures* $z \neq x_i$. *Project:* $z \leftarrow \mathrm{clamp}(z, \ell, u)$.
*Greedy refinement (one step). With* $g = z - x_i$, $x^{\mathrm{ref}} = \mathrm{clamp}(x_i + \beta g, \ell, u)$, $\beta \in (0, 1]$*; greedy selection against the snapshot* $(x_i^0, f_i^0)$.
*Stagnation and micro-restarts. If no* $y_i$ *improves, stagnation counter* $s \uparrow$*; if* $s \geq \tau$*, restart worst* $m = \lfloor \rho N \rfloor$ *individuals by*

$$x_{i,j} \sim \mathcal{N}\big(x_j^\star, \sigma^2 (u_j - \ell_j)^2\big) \text{ with prob. } \pi, \quad \text{else } x_{i,j} \sim \mathcal{U}(\ell_j, u_j),$$

then project $x_i \leftarrow \mathrm{clamp}(x_i, \ell, u)$.
*Termination.* Primary: $\mathrm{FE} \geq \mathrm{FE}_{\max}$; secondary: $t \geq I_{\max}$.

TRIDENT-DE is a population-based, derivative-free optimizer designed for box-constrained minimization of a continuous objective $f : S \to \mathbb{R}$ over $S = [\ell, u] = \prod_{j=1}^{n} [\ell_j, u_j]$. At iteration $t$, the algorithm maintains a population $\{x_i^{(t)}\}_{i=1}^{N} \subset S$ with fitness values $y_i^{(t)} = f\Big(x_i^{(t)}\Big)$. The incumbent elite is

$$i^\star = \arg\min_i y_i^{(t)}, \qquad x^\star = x_{i^\star}^{(t)}, \qquad f^\star = f(x^\star).$$

An elite archive $A$ of capacity $\kappa$ stores the best solutions seen so far (ties resolved by $f$) to support pbest sampling, feasibility is enforced throughout by componentwise projection $\mathrm{clamp}(x, \ell, u)$, where for each coordinate $j$ we set $x_j \leftarrow \min\{\max\{x_j, \ell_j\}, u_j\}$.

Initialization.

Each coordinate is drawn independently as $x_{i,j}^{(0)} \sim \mathcal{U}(\ell_j, u_j)$; then $y_i^{(0)} = f\Big(x_i^{(0)}\Big)$ is evaluated, the elite $x^\star$ is set, and the archive is seeded as $A \leftarrow \{x^\star\}$. This uniform seeding spreads initial mass across $S$ without imposing structural priors on $f$.

Per-iteration control flow.

At the start of iteration $t$, the elite is refreshed so that all subsequent operators are anchored to the most recent best. For each individual $i$, a rollback snapshot $(x_i^0, f_i^0) = (x_i^{(t)}, y_i^{(t)})$ is taken to guarantee non-worsening replacement. A trial-vector generator $\mathrm{op} \in \{\mathrm{best}/1, \mathrm{current\text{-}to\text{-}best}/1, \mathrm{pbest}/1, \mathrm{none}\}$ is selected by a categorical draw with probabilities $(r, q, p, 1-(r+q+p))$. This triad yields complementary pressures: *best/1* concentrates exploitation around $x^\star$; *current-to-best/1* steers $x_i$ toward $x^\star$ while retaining a differential term, *pbest/1* exploits $A \cup \{x^\star\}$ to distribute attraction over multiple high-quality anchors, the *none* branch stabilizes dynamics when parameter jitter is aggressive.

Light self-adaptation.

Control parameters are perturbed at the individual level using one Gaussian deviate per parameter:

$$F_i = \mathrm{clip}(F + \lambda_F\,\xi_F,\,0,\,2), \qquad C_i = \mathrm{clip}(C + \lambda_C\,\xi_C,\,0,\,1),$$

with $\xi_F, \xi_C \sim \mathcal{N}(0,1)$ independent and $\lambda_F, \lambda_C > 0$ controlling jitter amplitude. This preserves evaluation efficiency while adapting to local roughness.

Donor formation, crossover and projection.

With mutually distinct indices $r_1 \neq r_2 \neq i$ drawn uniformly from $\{1,\dots,N\}$, the donor $v$ is

$$\begin{aligned}
\textbf{best/1:} \quad & v = x^\star + F_i\,(x_{r_1}^{(t)} - x_{r_2}^{(t)}),\\
\textbf{current-to-best/1:} \quad & v = x_i^{(t)} + F_i\,(x^\star - x_i^{(t)}) + F_i\,(x_{r_1}^{(t)} - x_{r_2}^{(t)}),\\
p\textbf{best/1:} \quad & p^\star \sim \mathrm{Unif}\big(A \cup \{x^\star\}\big), \quad v = p^\star + F_i\,(x_{r_1}^{(t)} - x_{r_2}^{(t)}),
\end{aligned}$$

and $v = x_i^{(t)}$ if op = none. Binomial crossover with rate $C_i$ forms $z$ from $(v, x_i^{(t)})$, forcing one dimension $j_{\mathrm{rand}}$ from $v$ to ensure $z \neq x_i^{(t)}$; feasibility is restored by $z \leftarrow \mathrm{clamp}(z, \ell, u)$.

One-step greedy refinement and acceptance.

Let $g = z - x_i^{(t)}$. A low-cost, one-evaluation line refinement proposes

$$x^{\mathrm{ref}} = \mathrm{clamp}\big(x_i^{(t)} + \beta\,g,\,\ell,\,u\big), \qquad \beta \in (0,1],$$

and evaluates $f(x^{\mathrm{ref}})$. If $f(x^{\mathrm{ref}}) < f_i^0$, we accept $(x_i^{(t+1)}, y_i^{(t+1)}) = (x^{\mathrm{ref}},\, f(x^{\mathrm{ref}}))$; otherwise we evaluate the raw trial once, $f(z)$, accepting $z$ if $f(z) < f_i^0$ and rolling back to $(x_i^0, f_i^0)$ otherwise. Whenever a replacement improves the global best, we set $x^\star \leftarrow x_i^{(t+1)}$, update $f^\star$, and update the archive $A$ (insert if $|A| < \kappa$, else replace the worst).

Stagnation and adaptive micro-restarts.

A stagnation counter $s$ increments when no $y_i$ improves within an iteration; otherwise it resets. If $s \geq \tau$, we restart the worst $m = \lfloor \rho N \rfloor$ individuals. For each restarted index $i$, with probability $\pi$ we sample an elite-centred Gaussian kick

$$x_{i,j} \sim \mathcal{N}\big(x_j^\star,\,\sigma^2\,(u_j - \ell_j)^2\big) \quad \text{independently for } j = 1,\dots,n,$$

and with probability $1 - \pi$ we reinitialize uniformly $x_{i,j} \sim \mathcal{U}(\ell_j, u_j)$; in both cases we project with $x_i \leftarrow \mathrm{clamp}(x_i, \ell, u)$ and refresh $y_i = f(x_i)$.

Budget and ordering.

Termination is governed primarily by the evaluation budget $\mathrm{FE} \geq \mathrm{FE}_{\max}$ and secondarily by an iteration cap $t \geq I_{\max}$. The ordering elite refresh, operator selection, parameter jitter, donor formation, crossover, projection, greedy refinement, fallback raw-trial, acceptance/archive update, stagnation accounting, and (if needed) micro-restart ensures that refinement reuses a precomputed direction, projection preserves feasibility at every stage, and diversity is injected only under verified stagnation.

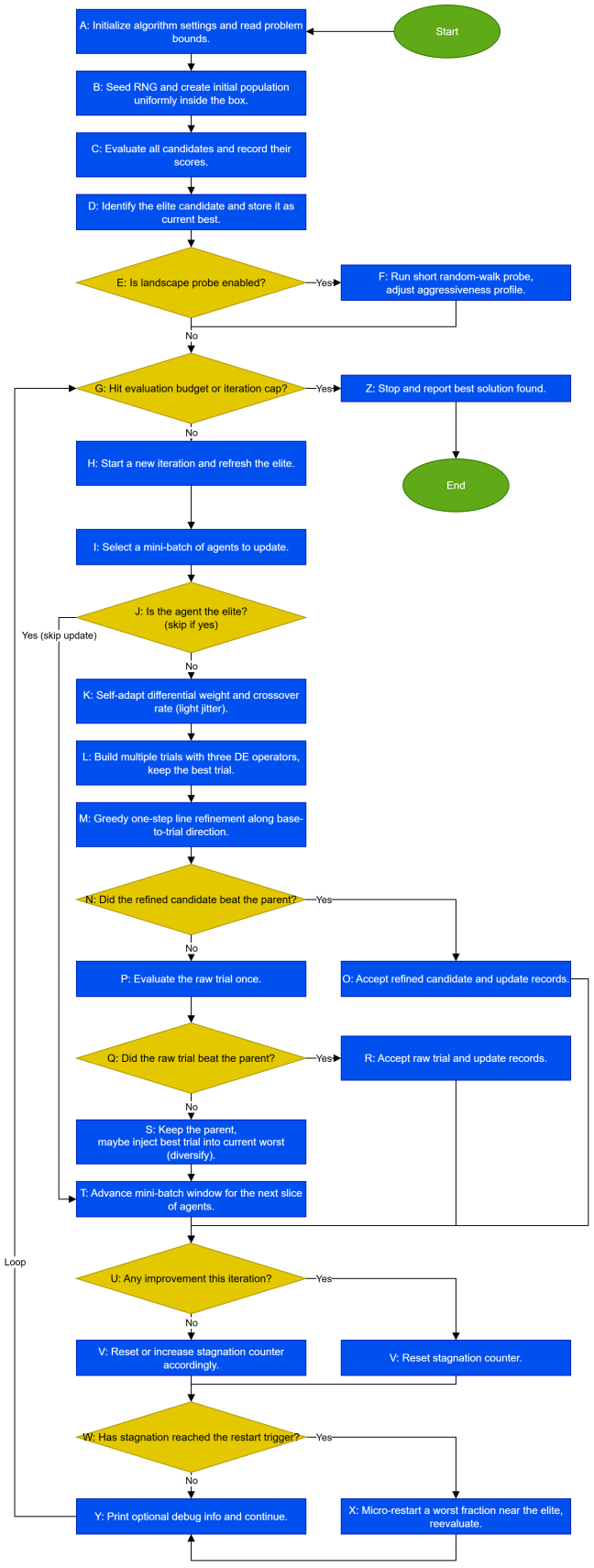


**Figure 1.** TRIDENT-DE flowchart: triple-operator DE with greedy refinement and adaptive micro-restarts

As shown in Figure 1, after initialization and elite refresh, each agent undergoes operator selection, parameter jitter, trial construction, and greedy line refinement, followed if necessary by a single raw-trial evaluation. Iteration-level progress is assessed at node U, to avoid ambiguity, the "Yes" and "No" branches lead to separate actions V (reset stagnation counter) and Y (increase stagnation counter) which both feed into W (restart trigger). When the trigger fires, micro-restarts (X) rejuvenate a worst fraction near the elite (or uniformly), after which the loop returns to the main termination check. This organization clarifies control flow, emphasizes the low-cost refinement step, and shows precisely how stagnation governs diversity injection.

## 3. Experimental setup and benchmark results

### *3.1. Setup*

Table 1 summarizes the core settings of TRIDENT-DE, grouping the population size, the box bounds, and the default DE controls ($F$, $C$) together with the jDE-style self-adaptation (resampling probabilities and sampling ranges). It also lists the hyper-parameters governing the triple trial-vector ensemble, the greedy line-refinement, and the adaptive micro-restart policy (restart fraction $\rho$, Gaussian kick scale $\sigma$, stagnation trigger $\tau$). Note that operator scheduling follows a round-robin (three operators) scheme in the manuscript, while the implementation uses a round-robin (three operators) to balance exploration and exploitation across iterations. The defaults $\mathrm{FE}_{\max} = 1.5 \cdot 10^5$ and $I_{\max} = 500$ standardize the computational budget across problems and act as termination criteria, with priority given to the evaluation budget (see Table 1)

**Table 1.** TRIDENT-DE parameters

| Name | Value | Description |
|---|---|---|
| $N$ | 100 | Population size |
| $n$ | problem | Problem dimension (from instance). |
| $[\ell, u]$ | from problem, fallback $[-1, 1]^n$ | Box bounds, fallback used if margins missing. |
| $F$ | $F^0 = 0.9$ | Baseline scale, per-individual $F_i$ (jDE-style control in code). |
| $C$ | $C^0 = 0.7$ | Baseline crossover, per-individual $C_i$ (jDE-style control in code). |
| $r, q, p$ | (round-robin) | Operator selection in manuscript, implementation uses 3-operator cycle. |
| $\tau$ | 18 | Stagnation trigger (no-improvement iterations before restart). |
| $\rho$ | 0.10 | Fraction of worst individuals to restart. |
| $\sigma$ | 0.20 | Gaussian kick scale at restart ($\times$ box range). |
| $\beta$ | {1.0, 0.5} | One-step greedy line-refine factors. |
| $\mathrm{FE}_{\max}$ | 150,000 | Evaluation-budget termination (code default). |
| $I_{\max}$ | 500 | Iteration cap (used in manuscript, not enforced by code). |
| $\alpha$ | 0.55 | Mini-batch ratio. |
| $t$ | 4 | Trials per agent. |
| $\tau_F$ | 0.10 | jDE resampling prob. for $F_i$. |
| $\tau_C$ | 0.10 | jDE resampling prob. for $C_i$. |
| $F_\ell, F_u$ | 0.1, 1.2 | Bounds for jDE resampling of $F_i$. |
| $C_\ell, C_u$ | 0.0, 0.95 | Bounds for jDE resampling of $C_i$. |
| $\varphi$ | 0.10 | Top-$p$ fraction for pbest/1. |

Table 2 reports the configurations of all competitor methods to ensure reproducibility and fairness with respect to population size and iteration budget. For each algorithm, we list its internal controls (e.g., the comprehensive-learning probability for CLPSO, population sizing and coefficients for CMA-ES, JADE-style parameters for EA4Eig, success-history memories and p-best ranges for mLSHADE_RL and UDE3, and adaptation schemes for SaDE) as used in our experiments. Harmonizing the population at $N = 100$ and the iteration cap at $I_{\max} = 500$ guarantees comparability, while per-method settings follow the literature and publicly available implementations.

**Table 2.** Parameters of other methods

| Name | Value | Description |
|---|---|---|
| $N$ | 100 | Population size for all methods |
| $I_{\max}$ | 500 | Maximum number of iterations for all methods |
| | **CLPSO** | |
| clProb | 0.3 | Comprehensive learning probability |
| cognitiveWeight | 1.49445 | Cognitive weight |
| inertiaWeight | 0.729 | Inertia weight |
| mutationRate | 0.01 | Mutation rate |
| socialWeight | 1.49445 | Social weight |
| | **CMA-ES** | |
| $N_{CMA-ES}$ | $4 + \lfloor 3 \cdot \log(dim) \rfloor$ | Population size |
| | **EA4Eig** | |
| archiveSize | 100 | Archive size for JADE-style mutation |
| eig_interval | 5 | Recompute eigenbasis every k iterations |
| maxCR | 1 | Upper bound for CR |
| maxF | 1 | Upper bound for F |
| minCR | 0 | Lower bound for CR |
| minF | 0.1 | Lower bound for F |
| pbest | 0.2 | p-best fraction (current-to-pbest/1) |
| tauCR | 0.1 | Self-adaptation prob. for CR |
| tauF | 0.1 | Self-adaptation prob. for F |
| | **mLSHADE_RL** | |
| archiveSize | 500 | Archive size |
| memorySize | 10 | Success-history memory size (H) |
| minPopulation | 4 | Minimum population size |
| pmax | 0.2 | Maximum p-best fraction |
| pmin | 0.05 | Minimum p-best fraction |
| | **SaDE** | |
| crSigma | 0.1 | Std for CR sampling |
| fGamma | 0.1 | Scale for Cauchy F sampling |
| initCR | 0.5 | Initial CR mean |
| initF | 0.7 | Initial F mean |
| learningPeriod | 25 | Iterations per adaptation window |
| | **UDE3** | |
| minPopulation | 4 | Minimum population size. |
| memorySize | 10 | Success-history memory size (H). |
| archiveSize | 100 | Archive size. |
| pmin | 0.05 | Minimum p-best fraction. |
| pmax | 0.2 | Maximum p-best fraction. |

All experiments were conducted on a high-performance node featuring an AMD Ryzen 9 5950X CPU (16 cores, 32 threads) and 128 GB of DDR4 memory, running Debian Linux. The evaluation protocol was designed for statistical rigor and reproducibility: each benchmark function was executed 30 times independently, using distinct random seeds to capture the stochastic variability of the algorithms.

The proposed method and all baselines were implemented in optimized ANSI C++ and integrated into the open-source OPTIMUS framework [23]. The source code is hosted at https://github.com/itsoulos/GLOBALOPTIMUS (accessed September 25, 2025), ensuring transparency and reproducibility. Parameter settings exactly follow Tables 1 and 2. Build environment: Debian 12.12 with GCC 13.4.

The primary performance indicator is the average number of objective-function evaluations over 30 runs for each test function. In all ranking tables comparing solvers, best values are highlighted in green (1st place) and second-best values in blue (2nd place).

### *3.2. Benchmark functions*

Table 3 compiles the real-world optimization problems used in our evaluation. For each case, we report a brief description, the dimensionality and variable types (continuous/mixed-integer), the nature and count of constraints (inequalities/equalities), salient landscape properties (nonconvexity, multi-modality), as well as the evaluation budget and comparison criteria. The set spans, indicatively, mechanical design, energy scheduling, process optimization, and parameter estimation with black-box simulators, ensuring that conclusions extend beyond synthetic test functions. Where applicable, we also note any normalizations or constraint reformulations adopted for fair comparison.

**Table 3.** The real world benchmark functions used in the conducted experiments

| Problem | Formula | Dim | Constraints/Bounds |
|---|---|---|---|
| **Parameter Estimation for Frequency-Modulated Sound Waves** | $\min_{x\in[-6.4,6.35]6}\ f(x)=\frac{1}{N}\sum_{n=1}^{N}\left\|y(n;x)-y_{\text{target}}(n)\right\|^2$<br>$y(n;x)=x_0\sin\left(x_1 n+x_2\sin(x_3 n+x_4\sin(x_5 n))\right)$ | 6 | $x_i\in[-6.4,6.35]$ |
| **Lennard-Jones Potential (atoms: 10, 13, 38)** | $\min_{x\in\mathbb{R}^{3N-6}}\ f(x)=4\sum_{i=1}^{N-1}\sum_{j=i+1}^{N}\left[\left(\frac{1}{r_{ij}}\right)^{12}-\left(\frac{1}{r_{ij}}\right)^{6}\right]$ | 24, 43, 108 | $x_0\in(0,0,0)$<br>$x_1,x_2\in[0,4]$<br>$x_3\in[0,\pi]$<br>$x_{3k-3}$<br>$x_{3k-2}$<br>$x_i\in[-b_k,+b_k]$ |
| **Bifunctional Catalyst Blend Optimal Control** | $\frac{dx_1}{dt}=-k_1x_1,\ \frac{dx_2}{dt}=k_1x_1-k_2x_2+k_3x_2+k_4x_3,$<br>$\frac{dx_3}{dt}=k_2x_2,\ \frac{dx_4}{dt}=-k_4x_4+k_5x_5,$<br>$\frac{dx_5}{dt}=-k_3x_2+k_6x_4-k_5x_5+k_7x_6+k_8x_7+k_9x_5+k_{10}x_7$<br>$\frac{dx_6}{dt}=k_8x_5-k_7x_6,\ \frac{dx_7}{dt}=k_9x_5-k_{10}x_7$<br>$k_i(u)=c_{i1}+c_{i2}u+c_{i3}u^2+c_{i4}u^3$ | 1 | $u\in[0.6,0.9]$ |
| **Optimal Control of a Non-Linear Stirred Tank Reactor** | $J(u)=\int_0^{0.72}\left[x_1(t)^2+x_2(t)^2+0.1u^2\right]dt$<br>$\frac{dx_1}{dt}=-2x_1+x_2+1.25u+0.5\exp\left(\frac{x_1}{x_1+2}\right)$<br>$\frac{dx_2}{dt}=-x_2+0.5\exp\left(\frac{x_1}{x_1+2}\right)$<br>$x_1(0)=0.9,\quad x_2(0)=0.09,\ t\in[0,0.72]$ | 1 | $u\in[0,5]$ |
| **Tersoff Potential for model Si (B)** | $\min_{\mathbf{x}\in\Omega}f(\mathbf{x})=\sum_{i=1}^{N}E(\mathbf{x}_i)$<br>$E(\mathbf{x}_i)=\frac{1}{2}\sum_{j\neq i}f_c(r_{ij})\left[V_R(r_{ij})-B_{ij}V_A(r_{ij})\right]$<br>where $r_{ij}=\|\mathbf{x}_i-\mathbf{x}_j\|$, $V_R(r)=A\exp(-\lambda_1 r)$<br>$V_A(r)=B\exp(-\lambda_2 r)$<br>$f_c(r)$: cutoff function with $f_c(r)$: angle parameter | 30 | $x_1\in[0,4]$<br>$x_2\in[0,4]$<br>$x_3\in[0,\pi]$<br>$x_i\in\left[\frac{4(i-3)}{4},4\right]$ |
| **Tersoff Potential for model Si (C)** | $\min_{\mathbf{x}}\ V(\mathbf{x})=\sum_{i=1}^{N}\sum_{j>i}^{N}f_C(r_{ij})\left[a_{ij}f_R(r_{ij})+b_{ij}f_A(r_{ij})\right]$<br>$f_C(r)=\begin{cases}1, & r<R-D\\ \frac{1}{2}+\frac{1}{2}\cos\left(\frac{\pi(r-R+D)}{2D}\right), & \lvert r-R\rvert\le D\\ 0, & r>R+D\end{cases}$<br>$f_R(r)=A\exp(-\lambda_1 r)$<br>$f_A(r)=-B\exp(-\lambda_2 r)$<br>$b_{ij}=\left[1+(\beta^n)\zeta_{ij}^n\right]^{-1/(2n)}$<br>$\sum_{k\neq i,j}f_C(r_{ik})g(\theta_{ijk})\exp\left[\lambda_3^3(r_{ij}-r_{ik})^3\right]$ | 30 | $x_1\in[0,4]$<br>$x_2\in[0,4]$<br>$x_3\in[0,\pi]$<br>$x_i\in\left[\frac{4(i-3)}{4},4\right]$ |
| **Spread Spectrum Radar Polyphase Code Design** | $\min_{x\in X}\ f(x)=\max\{\lvert\varphi_1(x)\rvert,\lvert\varphi_2(x)\rvert,\ldots,\lvert\varphi_m(x)\rvert\}$<br>$X=\{x\in\mathbb{R}^n\mid 0\le x_j\le 2\pi,\ j=1,\ldots,n\}m=2n-1$<br>$\varphi_j(x)=\begin{cases}\sum_{k=1}^{n-j}\cos(x_k-x_{k+j}) & \text{for } j=1,\ldots,n-1\\ n & \text{for } j=n\\ \varphi_{2n-j}(x) & \text{for } j=n+1,\ldots,2n-1\end{cases}$<br>$\varphi_j(x)=\sum_{k=1}^{n-j}\cos(x_k-x_{k+j}),\quad j=1,\ldots,n-1$<br>$\varphi_n(x)=n,\ \varphi_{n+\ell}(x)=\varphi_{n-\ell}(x),\quad \ell=1,\ldots,n-1$ | 20 | $x_j\in[0,2\pi]$ |
| **Transmission Network Expansion Planning** | $\min\sum_{l\in\Omega}c_l n_l+W_1\sum_{l\in OL}\lvert f_l-\bar{f}_l\rvert+W_2\sum_{l\in\Omega}\max(0,n_l-\bar{n}_l)$<br>$Sf=g-d$<br>$f_l=\gamma_l n_l\Delta\theta_l,\quad\forall l\in\Omega$<br>$\lvert f_l\rvert\le\bar{f}_l n_l,\quad\forall l\in\Omega$<br>$0\le n_l\le\bar{n}_l,\quad n_l\in\mathbb{Z},\quad\forall l\in\Omega$ | 7 | $0\le n_i\le\bar{n}_l$<br>$n_i\in\mathbb{Z}$ |
| **Electricity Transmission Pricing** | $\min_x\ f(x)=\sum_{i=1}^{N_g}\left(\frac{C_i^{gen}}{P_i^{gen}}-R_i^{gen}\right)^2+\sum_{j=1}^{N_d}\left(\frac{C_j^{load}}{P_j^{load}}-R_j^{load}\right)^2$<br>$\sum_j GD_{i,j}+\sum_j BT_{i,j}=P_i^{gen},\quad\forall i$<br>$\sum_i GD_{i,j}+\sum_i BT_{i,j}=P_j^{load},\quad\forall j$<br>$GD_{i,j}^{max}=\min(P_i^{gen}-BT_{i,j},\ P_j^{load}-BT_{i,j})$ | 126 | $GD_{i,j}\in[0,GD_{i,j}^{max}]$ |
| **Circular Antenna Array Design** | $\min_{r_1,\ldots,r_6,\varphi_1,\ldots,\varphi_6}\ f(\mathbf{x})=\max_{\theta\in\Omega}AF(\mathbf{x},\theta)$<br>$AF(\mathbf{x},\theta)=\left\lvert\sum_{k=1}^{6}\exp\left(j\left[2\pi r_k\cos(\theta-\theta_k)+\varphi_k\frac{\pi}{180}\right]\right)\right\rvert$ | 12 | $r_k\in[0.2,1]$<br>$\varphi_k\in[-180,180]$ |
| **Cassini 2: Spacecraft Trajectory Optimization Problem** | $x=[t_0,\ \Delta t_1,\ldots,\Delta t_5,\ p_1,\ldots,p_4]^\top,$<br>$\min_x J(x)=\Delta v_{\text{launch}}+\sum_{\ell=1}^{4}\Delta v_\ell^{\text{DSM}}+\Delta v_{\text{arrival}},$<br>$E\ \to\ V\ \to\ E\ \to\ V\ \to\ J\ \to\ S$<br>$t_0\in[850,\ 2000],\qquad\Delta t_\ell\in[20,\ 1200],\qquad p_\ell\in[1.0,\ 10.0].$ | 10 | $r_{p,\ell}\ge R_{p_\ell}+h_{\min,P_\ell},$<br>$\delta_\ell\le\delta_{\max,P_\ell},$<br>$t_0^{\min}\le t_0\le t_0^{\max},$<br>$\Delta t_\ell^{\min}\le\Delta t_\ell\le\Delta t_\ell^{\max}.$ |
| **Wireless Coverage Antenna Placement** | $x_i,\ y_i\in\mathbb{R}\quad(\text{position}),P_i\in\mathbb{R}_{\ge 0}\quad(\text{transmission power}).$<br>$S_{iu}(x_i,y_i,P_i)\ =\ \frac{G\,P_i}{\left((x_i-x_u)^2+(y_i-y_u)^2\right)^{\alpha/2}+\varepsilon},$<br>$\min_{x,y,P}\ \underbrace{\sum_{u\in\mathcal{U}}\left[\tau-S_u(x,P)\right]_+}_{\text{coverage deficiency}}+\lambda_P\sum_{i=1}^{N}P_i+,$<br>$\lambda_O\sum_{u\in\mathcal{U}}\sum_{i<j}\left[\min\{S_{iu},S_{ju}\}-\kappa\right]_+$<br>$S_u(x,P)\ =\ \max_{i=1,\ldots,N}\ S_{iu}(x_i,y_i,P_i).$ | 30 | $0\le x_i\le W,$<br>$0\le y_i\le H,$<br>$0\le P_i\le P_{\max}$ |
| **Dynamic Economic Dispatch 1** | $\min_{\mathbf{P}}\ f(\mathbf{P})=\sum_{t=1}^{24}\sum_{i=1}^{5}\left(a_iP_{i,t}^2+b_iP_{i,t}+c_i\right)$<br>$P_i^{\min}\le P_{i,t}\le P_i^{\max},\quad\forall i=1,\ldots,5,\ t=1,\ldots,24$<br>$\sum_{i=1}^{5}P_{i,t}=D_t,\quad\forall t=1,\ldots,24$<br>$P_{\min}=[10,20,30,40,50]$<br>$P_{\max}=[75,125,175,250,300]$ | 120 | $P_i^{\min}\le P_{i,t}\le P_i^{\max}$ |
| **Dynamic Economic Dispatch 2** | $\min_{\mathbf{P}}\ f(\mathbf{P})=\sum_{t=1}^{24}\sum_{i=1}^{9}\left(a_iP_{i,t}^2+b_iP_{i,t}+c_i\right)$<br>$P_i^{\min}\le P_{i,t}\le P_i^{\max},\quad\forall i=1,\ldots,5,\ t=1,\ldots,24$<br>$\sum_{i=1}^{5}P_{i,t}=D_t,\quad\forall t=1,\ldots,24$<br>$P_{\min}=[150,135,73,60,73,57,20,47,20]$<br>$P_{\max}=[470,460,340,300,243,160,130,120,80]$ | 216 | $P_i^{\min}\le P_{i,t}\le P_i^{\max}$ |
| **Static Economic Load Dispatch (1,2,3,4,5)** | $\min_{P_1,\ldots,P_{N_G}}\ F=\sum_{i=1}^{N_G}f_i(P_i)$<br>$f_i(P_i)=a_iP_i^2+b_iP_i+c_i,\quad i=1,2,\ldots,N_G$<br>$f_i(P_i)=a_iP_i^2+b_iP_i+c_i+\lvert e_i\sin(f_i(P_i^{\min}-P_i))\rvert$<br>$P_i^{\min}\le P_i\le P_i^{\max},\quad i=1,2,\ldots,N_G$<br>$\sum_{i=1}^{N_G}P_i=P_D+P_L$<br>$P_L=\sum_{i=1}^{N_G}\sum_{j=1}^{N_G}P_iB_{ij}P_j+\sum_{i=1}^{N_G}B_{0i}P_i+B_{00}$<br>$P_i-P_i^0\le UR_i\quad P_i^0-P_i\le DR_i$ | 6<br>13<br>15<br>40<br>140 | See Technical Report of CEC2011 |

### 3.3. Parameter sensitivity analysis of TRIDENT-DE

Following Lee et al.'s [24] parameter-sensitivity methodology, we construct a structured analysis to quantify responsiveness to parameter changes and the preservation of reliability across diverse operating regimes.

**Table 4.** Sensitivity analysis of the method parameters for the "Lennard-Jones Potential, Dim:10" problem

| Parameter | Value | Mean | Min | Max | Iters | Main effect range |
|---|---|---|---|---|---|---|
| $\tau$ | 12 | -27.0878 | -28.4225 | -24.0293 | 3240 | 0.0137 |
| | 18 | -27.0741 | -28.4225 | -23.2567 | 3240 | |
| | 30 | -27.0871 | -28.4225 | -23.0968 | 3240 | |
| $\rho$ | 0.05 | -27.0741 | -28.4225 | -23.0968 | 3240 | 0.0143 |
| | 0.1 | -27.0885 | -28.4225 | -23.1044 | 3240 | |
| | 0.2 | -27.0864 | -28.4225 | -23.6869 | 3240 | |
| $\sigma$ | 0.1 | -27.0913 | -28.4225 | -23.6906 | 3240 | 0.0138 |
| | 0.2 | -27.0803 | -28.4225 | -23.1044 | 3240 | |
| | 0.3 | -27.0775 | -28.4225 | -23.0968 | 3240 | |
| $t$ | 2 | -27.0823 | -28.4225 | -23.1044 | 3240 | 0.0066 |
| | 4 | -27.0861 | -28.4225 | -23.2567 | 3240 | |
| | 6 | -27.0842 | -28.4225 | -23.0968 | 3240 | |
| | 8 | -27.0794 | -28.4225 | -23.6906 | 3240 | |
| $\varphi$ | 0.06 | -27.0916 | -28.4225 | -23.0968 | 3240 | 0.0145 |
| | 0.1 | -27.0803 | -28.4225 | -23.2567 | 3240 | |
| | 0.18 | -27.0771 | -28.4225 | -23.1044 | 3240 | |

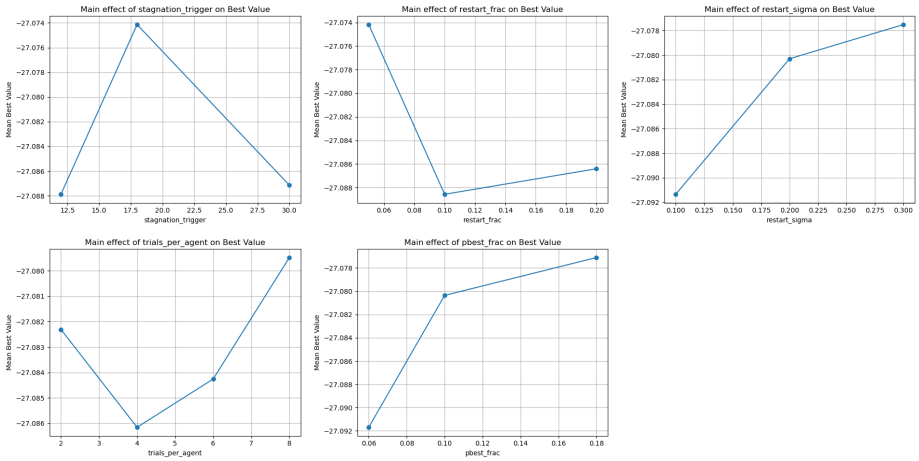


**Figure 2.** Graphical representation of $\tau$, $\rho$, $\sigma$, $t$ and $\varphi$ for the "Lennard-Jones Potential, Dim:10" problem

**Table 5.** Sensitivity analysis of the method parameters for the "Tersoff Potential for model Si (C)" problem

| Parameter | Value | Mean | Min | Max | Iters | Main effect range |
|---|---|---|---|---|---|---|
| $\tau$ | 12 | -31.6851 | -34.1571 | -27.5111 | 3240 | 0.0171 |
| | 18 | -31.6897 | -34.5056 | -27.9642 | 3240 | |
| | 30 | -31.6725 | -34.1820 | -28.0777 | 3240 | |
| $\rho$ | 0.05 | -31.6850 | -34.2058 | -27.6689 | 3240 | 0.0118 |
| | 0.1 | -31.6752 | -34.5056 | -28.2521 | 3240 | |
| | 0.2 | -31.6870 | -34.2775 | -27.5111 | 3240 | |
| $\sigma$ | 0.1 | -31.6830 | -34.1571 | -27.5111 | 3240 | 0.0139 |
| | 0.2 | -31.6890 | -34.5056 | -28.0084 | 3240 | |
| | 0.3 | -31.6751 | -34.2775 | -27.6689 | 3240 | |
| $t$ | 2 | -31.6994 | -34.2775 | -27.6689 | 3240 | 0.0524 |
| | 4 | -31.7036 | -34.5056 | -28.0084 | 3240 | |
| | 6 | -31.6753 | -34.1820 | -27.9642 | 3240 | |
| | 8 | -31.6512 | -34.1365 | -27.5111 | 3240 | |
| $\varphi$ | 0.06 | -31.6887 | -34.1365 | -27.5111 | 3240 | 0.0127 |
| | 0.1 | -31.6825 | -34.1820 | -28.0777 | 3240 | |
| | 0.18 | -31.6760 | -34.5056 | -27.6689 | 3240 | |

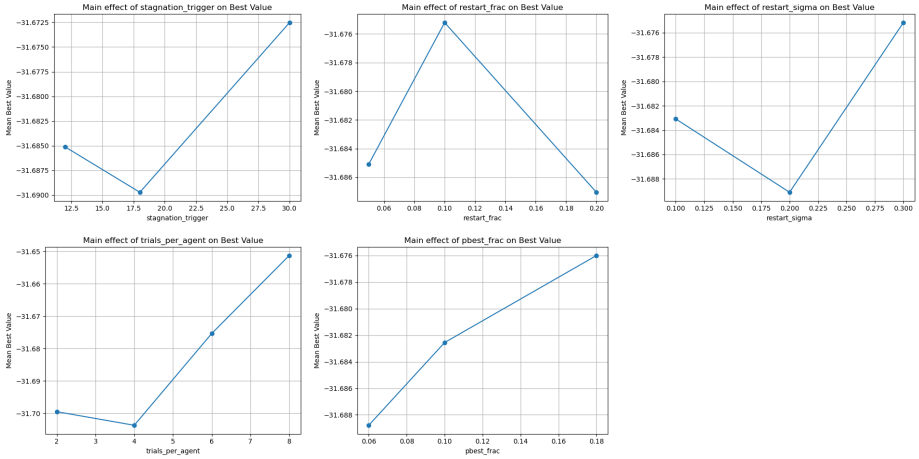


**Figure 3.** Graphical representation of $\tau$, $\rho$, $\sigma$, $t$ and $\varphi$ for the "Tersoff Potential for model Si (C)" problem

**Table 6.** Sensitivity analysis of the method parameters for the "Static Economic Load Dispatch 1" problem

| Parameter | Value | Mean | Min | Max | Iters | Main effect range |
|---|---|---|---|---|---|---|
| $\tau$ | 12 | 2977.7669 | 2967.2491 | 3002.3335 | 3240 | 0.3580 |
| | 18 | 2977.5983 | 2967.2491 | 3039.8430 | 3240 | |
| | 30 | 2977.9563 | 2967.2491 | 3167.0430 | 3240 | |
| $\rho$ | 0.05 | 2977.7981 | 2967.2491 | 3167.0430 | 3240 | 0.1440 |
| | 0.1 | 2977.8338 | 2967.2491 | 3039.8430 | 3240 | |
| | 0.2 | 2977.6897 | 2967.2491 | 3039.8430 | 3240 | |
| $\sigma$ | 0.1 | 2977.7085 | 2967.2491 | 3167.0430 | 3240 | 0.1282 |
| | 0.2 | 2977.8367 | 2967.2491 | 3031.7766 | 3240 | |
| | 0.3 | 2977.7764 | 2967.2491 | 3039.8430 | 3240 | |
| $t$ | 2 | 2977.6721 | 2967.2491 | 3039.8430 | 3240 | 0.1995 |
| | 4 | 2977.7556 | 2967.2491 | 3039.8430 | 3240 | |
| | 6 | 2977.7959 | 2967.2491 | 3039.8430 | 3240 | |
| | 8 | 2977.8717 | 2967.2491 | 3167.0430 | 3240 | |
| $\varphi$ | 0.06 | 2977.9287 | 2967.2491 | 3039.8430 | 3240 | 0.3351 |
| | 0.1 | 2977.7994 | 2967.2491 | 3167.0430 | 3240 | |
| | 0.18 | 2977.5935 | 2967.2491 | 3031.7766 | 3240 | |

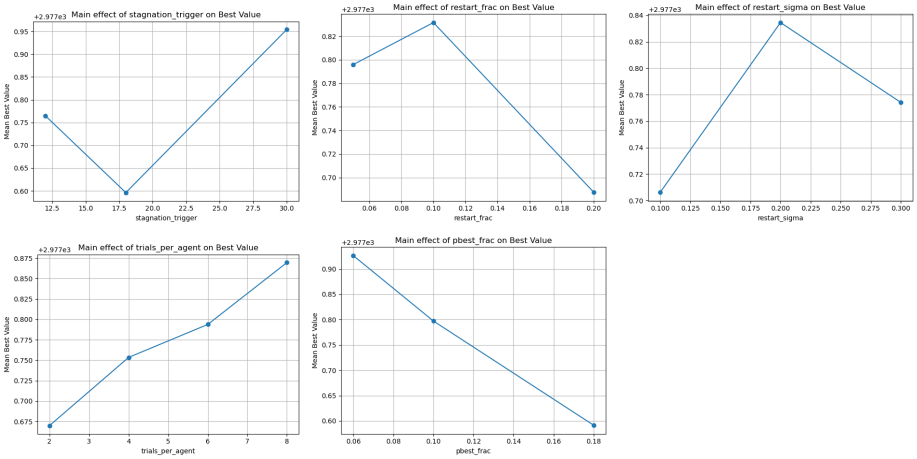


**Figure 4.** Graphical representation of $\tau$, $\rho$, $\sigma$, $t$ and $\varphi$ for the "Static Economic Load Dispatch 1" problem

The parameter sensitivity study probes the stability of TRIDENT-DE under controlled variations of key hyperparameters and quantifies whether reliability is preserved across heterogeneous operating conditions. We focus on the stagnation counter before restart $\tau$, the restart fraction $\rho$, the elite-centred Gaussian kick scale $\sigma$ at restart, the number of trials per agent $t$, and the top-p fraction $\varphi$ that governs the pbest/1 sampling. Each factor is swept over representative values around the defaults in Table 1 while the remaining factors are kept fixed, and we record the impact on mean performance, extrema, and the main-effect range for three complementary test classes: a molecular Lennard-Jones cluster at $N$=10, the Tersoff potential for silicon (model B), and the Static Economic Load Dispatch (ELD-1) problem. This trio spans rugged, multimodal physical landscapes and heavily constrained industrial testbeds, thereby making observed trends transferable rather than instance-specific. For Lennard-Jones, perturbations around $\tau$ =12/18/30, $\rho$ =0.05/0.1/0.2, $\sigma$ =0.1/0.2/0.3, $t$ =2/4/6/8, and $\varphi$ =0.06/0.10/0.18 induce only minor shifts in mean objective value and very small main-effect ranges across all factors, indicating inherent robustness of the method in this multimodal setting. The tight concentration of means around ~-27.08 together with the lack of systematic movement in extremes suggests that the triple-operator ensemble, the mild jDE-style control on $F$ and $C$, and the one-step greedy line refinement

act as dampers against parameter oversensitivity, especially because the refinement reuses a precomputed direction at negligible variance cost. These observations are evident in Table 4 and Figure 2.

In the Tersoff-Si (model B) potential, the overall robustness pattern persists, with the number of trials per agent $t$ showing the most noticeable albeit still small effect on mean performance and main-effect range. Increasing $t$ slightly improves exploitation of promising directions, occasionally trading off diversity, yet exploration remains safeguarded by adaptive micro-restarts, so the dynamics do not collapse. The gentle drift in mean with $t$ does not overturn the defaults of Table 1, whereas $\rho$ and $\sigma$ exert only marginal influence within the probed ranges, underscoring that restarts serve as a safety valve rather than a dominant driver. The quantitative evidence is given in Table 5 and Figure 3.

The picture changes more distinctly for ELD-1. Here, the lack of time coupling removes inter-temporal interactions, yet feasibility remains tight due to the power-balance equality and unit output bounds. Depending on the presence of valve-point effects, the landscape can be markedly nonconvex, with ripple-like undulations around local extrema. In this setting, the stagnation threshold $\tau$ still acts as a reliable trigger for rejuvenation when the population gets trapped in shallow basins, but its relative influence is smaller than in dynamic DED-type problems because there are no time-linked plateaus reinforcing stagnation. By contrast, the top-p fraction $\varphi$ becomes the primary control knob: it governs how strongly the search is pulled toward p-best elites, mediating the trade-off between aggressive exploitation near top units and the preservation of diversity across alternative feasible corridors. Increasing $t$ (trials per agent) further improves the use of local directions without collapsing exploration, as adaptive micro-restarts with calibrated $\rho$ and $\sigma$ inject gentle diversity whenever stagnation is detected. The results in Table 6 and the corresponding figure 4 indicate that defaults around $\tau \approx 18$ and $\varphi \approx 0.10$ are safe operating points for ELD-1, small local retunings of these two parameters can yield more stable quality jumps when valve-point ripples make the landscape more "toothed," without requiring adjustments to $\rho$ and $\sigma$ beyond the probed ranges.

Taken together, the sensitivity profile shows that the defaults in Table 1 are well-balanced across diverse problems: $\rho$ and $\sigma$ regulate a gentle injection of diversity without disrupting exploitation, $\varphi$ shapes the attraction lattice of pbest/1 across multiple elites, and $t$ enhances the utility of the already computed direction $z \to x\top$ at modest additional cost. The small main-effect ranges observed in Lennard-Jones and Tersoff confirm that the triple-operator design, combined with light jDE-style jitter on $F$ and $C$, yields a self-stabilising regime in which parameter effects are largely second-order. Conversely, in heavily constrained energy scheduling, $\tau$ and $\varphi$ become active control knobs, consistent with a landscape featuring broad plateaus and tight feasibility margins. The practical implication is twofold: first, the proposed defaults deliver portable reliability with minimal pre-tuning, second, when constraints dominate, a narrow local retuning of $\tau$ and $\varphi$ around their nominal values preserves the best search rate without sacrificing stability. These conclusions align with the architecture of TRIDENT-DE, where interactions among three trial generators, one-step greedy refinement, and adaptive micro-restarts distribute the burden of adaptation and, as a result, insulate the system from sharp nonlinearities in any single hyperparameter.

### *3.4. Analysis of Complexity of TRIDENT-DE*

Below we provide a bullet-style specification of two real-world optimization problems adopted as representative testbeds for the time-complexity and scaling analysis of the proposed method, we summarise the key decision variables, admissible bounds/domains, and objective functions, and explicitly note relevant modeling assumptions and feasibility penalty terms, so that the ensuing bullets serve as a quick "map" of practical constraints and goals prior to the runtime evaluation.

- **GasCycle Thermal Cycle**

Vars: $\boldsymbol{x} = [T_1, T_3, P_1, P_3]^\top$. $r = P_3/P_1,\ \gamma = 1.4$.

$$\eta(\boldsymbol{x}) = 1 - r^{-(\gamma-1)/\gamma}\,\frac{T_1}{T_3}, \qquad \min_{\boldsymbol{x}} f(\boldsymbol{x}) = -\eta(\boldsymbol{x}).$$

Bounds: $300 \le T_1 \le 1500,\ 1200 \le T_3 \le 2000,\ 1 \le P_1, P_3 \le 20$.
Penalty: infeasible $\Rightarrow f = 10^{20}$.

- **Tandem Space Trajectory** (MGA-1DSM, EVEEJ + 2×Saturn)
  Vars **($D$=18):** $\boldsymbol{x} = [t_0, T_1, T_2, T_3, T_4, T_{5A}, T_{5B}, s_1, s_2, s_3, s_4, s_{5A}, s_{5B}, r_p, k_{A1}, k_{A2}, k_{B1}, k_{B2}]^\top$.

$$\begin{aligned}
&7000 \le t_0 \le 10000,\\
&30 \le T_1 \le 500,\ 30 \le T_2 \le 600,\ 30 \le T_3 \le 1200,\\
&30 \le T_4 \le 1600,\ 30 \le T_{5A}, T_{5B} \le 2000,\\
&0 \le s_{1..4}, s_{5A}, s_{5B}, r_p, k_{A1}, k_{A2}, k_{B1}, k_{B2} \le 1.
\end{aligned}$$

Objective:

$$\min_{\boldsymbol{x}}\ \Delta V_{\text{tot}} = \Delta V_{\text{launch}}(T_1) + \Delta V_{\text{legs}}(T_1{:}T_4) + \Delta V_A + \Delta V_B + \Delta V_{\text{DSM}}(\boldsymbol{s}, r_p) - G_{\text{GA}} - G_J + P_{\text{hard}} +$$

$$P_{\text{soft}} = \beta \max\Big\{0,\ (T_1 + \cdots + T_4 + \tfrac{1}{2}(T_{5A}+T_{5B})) - 3500\Big\}.$$

Notes: $\Delta V_{\text{launch}}$ decreases (log-like) in $T_1$ ($\ge$ 6 km/s floor), leg/branch costs decrease with TOF.

The time-complexity Figure 5 reveals an almost linear growth of wall-clock time with respect to problem size (40-400) for both GasCycle Thermal Cycle and Tandem Space Trajectory. The monotonic trend and near-constant increments per size step indicate that the proposed architecture scales effectively with $O(n)$ in the investigated size parameter, with no signs of exponential or strongly super-linear behavior. Across the two cases, Tandem Space Trajectory consistently exhibits slightly higher times, which is naturally explained by a larger per-evaluation cost of the underlying simulator/objective in that domain. In other words, the dominant contributor to total runtime is the evaluation cost, while the search mechanism itself preserves an approximately constant slope with respect to size. The absence of kinks or abrupt escalations at larger sizes further suggests that components such as the triple trial-vector ensemble, the one-step greedy line refinement, and the adaptive micro-restarts do not introduce hidden overhead that would manifest as degraded asymptotic scaling. Practically, the method remains predictable and efficient as the problem grows, with performance primarily governed by the problem-dependent evaluation burden. The mild, roughly constant offset between the two benchmarks over the 40-400 range reinforces the view that this is a domain-dependent additive cost rather than a change in the algorithm's scaling rate. Overall, the evidence supports a favorable scaling profile: linear complexity in the examined size parameter, stability under heavier loads, and a clean separation between a stable algorithmic overhead and the variable evaluation cost imposed by each application.

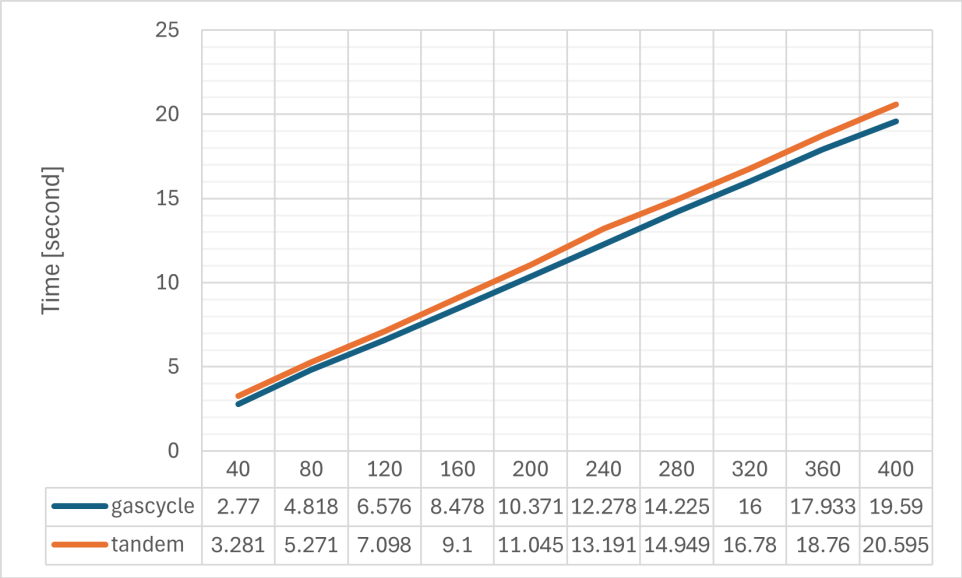


| | 40 | 80 | 120 | 160 | 200 | 240 | 280 | 320 | 360 | 400 |
|---|---|---|---|---|---|---|---|---|---|---|
| gascycle | 2.77 | 4.818 | 6.576 | 8.478 | 10.371 | 12.278 | 14.225 | 16 | 17.933 | 19.59 |
| tandem | 3.281 | 5.271 | 7.098 | 9.1 | 11.045 | 13.191 | 14.949 | 16.78 | 18.76 | 20.595 |

**Figure 5.** Time scaling under a fixed iteration budget

### *3.5. Comparative performance analysis of TRIDENT-DE*

This section introduces the experimental component that assesses the proposed method across alternative configurations and problem sets, emphasizing behavioral consistency and reproducibility. Table 7 compiles the corresponding comparative figures and summary evaluation metrics.

**Table 7.** Comparison Based on Best and Mean after 1.5e+5 FEs

| | TRIDENT-DE | UDE3 | EA4Eig | mLSHADE_RL | SaDE | CMA-ES | jDE | CLPSO |
|---|---|---|---|---|---|---|---|---|
| | Best/Mean | Best/Mean | Best/Mean | Best/Mean | Best/Mean | Best/Mean | Best/Mean | Best/Mean |
| **Lennard-Jones** | -28.42253189 | -17.60964115 | -22.47842596 | -28.42252711 | -22.86077544 | -28.42253189 | -15.91366007 | -16.59269921 |
| **Potential (10 atoms)** | -27.19833972 | -16.33758634 | -19.48663385 | -23.77189104 | -21.22806787 | -27.52754934 | -13.75563015 | -13.55503647 |
| **Lennard-Jones** | -41.39220729 | -21.90945922 | -28.01101572 | -40.6992486 | -29.31393114 | -44.32680142 | -18.77073675 | -18.00250514 |
| **Potential (13 atoms)** | -39.14390841 | -19.49372047 | -24.58810405 | -30.67706246 | -27.48874237 | -41.44245617 | -15.4243072 | -15.86691988 |
| **Lennard-Jones** | -125.1886792 | -2.015038465 | -55.05415428 | -120.0680452 | -68.91313107 | -167.7369019 | 9186.25096 | 330.9934848 |
| **Potential (38 atoms)** | -107.1751456 | 140.2211284 | -3.350181902 | -73.95117658 | -45.80265994 | -163.6091673 | 9186.25096 | 1087.035295 |
| **Tersoff Potential** | -28.93480467 | -25.43447342 | -26.90746941 | -28.12281867 | -26.65687822 | -28.33045002 | -24.75133772 | -22.67387001 |
| **for model Si (B)** | -27.70615763 | -23.30318979 | -24.69059932 | -25.49977206 | -25.27422603 | -27.38991233 | -22.94168766 | -21.21150428 |
| **Tersoff Potential** | -33.8820283 | -29.30227462 | -30.88865174 | -31.70444684 | -30.94469385 | -32.50963421 | -29.44789882 | -26.88039528 |
| **for model Si (C)** | -31.91749393 | -27.53891341 | -29.0199918 | -29.44303263 | -29.70029831 | -31.53772845 | -29.44789882 | -24.653633 |
| **Parameter Estimation for** | 0.116157535 | 0 | 0.15272453 | 0.116157535 | 0.148007602 | 0.210122687 | 0 | 0.131483748 |
| **Frequency-Modulated Sound Waves** | 0.134324544 | 0.103406319 | 0.213099692 | 0.208210846 | 0.148007602 | 0.267329914 | 0.132539923 | 0.212498169 |
| **Circular Antenna** | 0.006809638 | 0.006809665 | 0.006809638 | 0.006809662 | 0.006814682 | 0.007253731 | 0.00681715 | 0.006933401 |
| **Array Design** | 0.006809683 | 0.006817385 | 0.006809638 | 0.006825338 | 0.00790701 | 0.008755359 | 0.006835764 | 0.051815518 |
| **Spread Spectrum Radar** | 0.014426836 | 0.953872709 | 0.601567824 | 0.074552911 | 0.550837019 | 0.062519409 | 1.005739785 | 0.860294378 |
| **Polyphase Code Design** | 0.26254527 | 1.206577385 | 0.869257599 | 0.535028919 | 0.803527605 | 0.197713522 | 1.331416957 | 1.273200439 |
| **Cassini 2: Spacecraft Trajectory** | 0 | 0.000926598 | 0 | 0 | 0.039231105 | 0 | 0.000026961 | 1.22633022 |
| **Optimization Problem** | 0.000011205 | 0.008206106 | 0 | 0.00001729 | 0.070230417 | 5.929143722 | 0.000285411 | 3.639687905 |
| **Wireless Coverage** | 0.946350736 | 0.946350736 | 0.946655032 | 0.946350736 | 0.946361987 | 1.18939375 | 0.946350736 | 0.946365969 |
| **Antenna Placement** | 0.94662124 | 0.946502884 | 0.946659575 | 0.946875107 | 0.946688757 | 1.190699803 | 0.946401452 | 0.946727502 |
| **Transmission Network** | 4.485304003 | 4.485295106 | 4.485292926 | 4.485292926 | 4.485299525 | 4.485292926 | 4.485292926 | 4.486699087 |
| **Expansion Planning** | 4.485292926 | 4.485304003 | 4.485292926 | 4.485292926 | 4.485311924 | 4.485292948 | 4.485292926 | 4.495857336 |
| **Dynamic** | 130850.0389 | 130693.5423 | 130694.29 | 130882.0646 | 131010.8769 | 130650.9354 | 131225.2453 | 131834.4235 |
| **Economic Dispatch 1** | 130931.1074 | 130717.6052 | 130862.9893 | 130955.331 | 131099.1959 | 130654.2758 | 131225.2453 | 132151.5397 |
| **Dynamic** | 165980.9574 | 164946.164 | 172067.4426 | 167519.3281 | 167908.0605 | 165847.1092 | 186121.2812 | 177120.3822 |
| **Economic Dispatch 2** | 166478.1534 | 165614.9256 | 172931.6964 | 168275.5429 | 168495.9731 | 166233.691 | 190793.5621 | 178190.4198 |
| **Static Economic** | 2967.249196 | 2967.249196 | 2979.803369 | 2967.249196 | 2967.249196 | 2967.249586 | 2967.249196 | 2967.249197 |
| **Load Dispatch 1** | 2975.721343 | 2976.057657 | 2979.803369 | 2976.956221 | 2976.139816 | 3108.931917 | 2967.659992 | 2973.33009 |
| **Static Economic** | 17879.73679 | 17864.69687 | 18006.65976 | 17882.28384 | 17892.38129 | 17960.84734 | 17867.57447 | 17910.47794 |
| **Load Dispatch 2** | 17928.65603 | 17890.83413 | 18063.12085 | 17950.15892 | 17958.94204 | 18077.58006 | 17992.09486 | 18089.83526 |
| **Static Economic** | 32367.57735 | 32367.57735 | 32415.80367 | 32367.57765 | 32376.02197 | 32645.34102 | 32391.64981 | 32384.85409 |
| **Load Dispatch 3** | 32440.87752 | 32400.86337 | 32573.03572 | 32491.57235 | 32491.28971 | 32867.1729 | 32476.58405 | 32532.19143 |
| **Static Economic** | 121071.4654 | 121066.9247 | 121197.2468 | 121085.9922 | 121195.4656 | 122350.1013 | 121234.0466 | 121328.7006 |
| **Load Dispatch 4** | 121422.9908 | 121197.2468 | 121545.1315 | 121308.5801 | 121517.4918 | 122957.6217 | 121526.7414 | 121541.4182 |
| **Static Economic** | 508663.8176 | 508661.3113 | 508872.6908 | 508851.668 | 508985.9092 | 508717.1467 | 511174.5326 | 509025.7426 |
| **Load Dispatch 5** | 508703.0424 | 508676.4938 | 508986.6092 | 508988.5396 | 509125.2079 | 508770.1661 | 562012.6548 | 509080.3439 |

**Table 8.** Detailed Ranking of Algorithms Based on Best after 1.5e+5 FEs

| | TRIDENT-DE | UDE3 | EA4Eig | mLSHADE_RL | SaDE | CMA-ES | jDE | CLPSO |
|---|---|---|---|---|---|---|---|---|
| Lennard-Jones Potential (10 atoms) | 1 | 6 | 5 | 3 | 4 | 1 | 8 | 7 |
| Lennard-Jones Potential (13 atoms) | 2 | 6 | 5 | 3 | 4 | 1 | 7 | 8 |
| Lennard-Jones Potential (38 atoms) | 2 | 6 | 5 | 3 | 4 | 1 | 8 | 7 |
| Tersoff Potential for model Si (B) | 1 | 6 | 4 | 3 | 5 | 2 | 7 | 8 |
| Tersoff Potential for model Si (C) | 1 | 7 | 5 | 3 | 4 | 2 | 6 | 8 |
| Parameter Estimation for Frequency-Modulated Sound Waves | 3 | 1 | 7 | 3 | 6 | 8 | 1 | 5 |
| Circular Antenna Array Design | 1 | 4 | 2 | 3 | 5 | 8 | 6 | 7 |
| Spread Spectrum Radar Polyphase Code Design | 1 | 7 | 5 | 3 | 4 | 2 | 8 | 6 |
| Cassini 2: Spacecraft Trajectory Optimization Problem | 1 | 6 | 1 | 1 | 7 | 1 | 5 | 8 |
| Wireless Coverage Antenna Placement | 1 | 1 | 7 | 1 | 5 | 8 | 1 | 6 |
| Transmission Network Expansion Planning | 7 | 5 | 1 | 1 | 6 | 1 | 1 | 8 |
| Dynamic Economic Dispatch 1 | 4 | 2 | 3 | 5 | 6 | 1 | 7 | 8 |
| Dynamic Economic Dispatch 2 | 3 | 1 | 6 | 4 | 5 | 2 | 8 | 7 |
| Static Economic Load Dispatch 1 | 1 | 1 | 8 | 1 | 1 | 7 | 1 | 6 |
| Static Economic Load Dispatch 2 | 3 | 1 | 8 | 4 | 5 | 7 | 2 | 6 |
| Static Economic Load Dispatch 3 | 1 | 1 | 7 | 3 | 4 | 8 | 6 | 5 |
| Static Economic Load Dispatch 4 | 2 | 1 | 5 | 3 | 4 | 8 | 6 | 7 |
| Static Economic Load Dispatch 5 | 2 | 1 | 5 | 4 | 6 | 3 | 8 | 7 |

**Table 9.** Detailed Ranking of Algorithms Based on Mean after 1.5e+5 FEs

| | TRIDENT-DE | UDE3 | EA4Eig | mLSHADE_RL | SaDE | CMA-ES | jDE | CLPSO |
|---|---|---|---|---|---|---|---|---|
| Lennard-Jones Potential (10 atoms) | 2 | 6 | 5 | 3 | 4 | 1 | 7 | 8 |
| Lennard-Jones Potential (13 atoms) | 2 | 6 | 5 | 3 | 4 | 1 | 8 | 7 |
| Lennard-Jones Potential (38 atoms) | 2 | 6 | 5 | 3 | 4 | 1 | 8 | 7 |
| Tersoff Potential for model Si (B) | 1 | 6 | 5 | 3 | 4 | 2 | 7 | 8 |
| Tersoff Potential for model Si (C) | 1 | 7 | 6 | 5 | 3 | 2 | 4 | 8 |
| Parameter Estimation for Frequency-Modulated Sound Waves | 3 | 1 | 7 | 5 | 4 | 8 | 2 | 6 |
| Circular Antenna Array Design | 2 | 3 | 1 | 4 | 6 | 7 | 5 | 8 |
| Spread Spectrum Radar Polyphase Code Design | 2 | 6 | 5 | 3 | 4 | 1 | 8 | 7 |
| Cassini 2: Spacecraft Trajectory Optimization Problem | 2 | 5 | 1 | 3 | 6 | 8 | 4 | 7 |
| Wireless Coverage Antenna Placement | 3 | 2 | 4 | 7 | 5 | 8 | 1 | 6 |
| Transmission Network Expansion Planning | 1 | 6 | 1 | 1 | 7 | 5 | 1 | 8 |
| Dynamic Economic Dispatch 1 | 4 | 2 | 3 | 5 | 6 | 1 | 7 | 8 |
| Dynamic Economic Dispatch 2 | 3 | 1 | 6 | 4 | 5 | 2 | 8 | 7 |
| Static Economic Load Dispatch 1 | 3 | 4 | 7 | 6 | 5 | 8 | 1 | 2 |
| Static Economic Load Dispatch 2 | 2 | 1 | 6 | 3 | 4 | 7 | 5 | 8 |
| Static Economic Load Dispatch 3 | 2 | 1 | 7 | 5 | 4 | 8 | 3 | 6 |
| Static Economic Load Dispatch 4 | 3 | 1 | 7 | 2 | 4 | 8 | 5 | 6 |
| Static Economic Load Dispatch 5 | 2 | 1 | 4 | 5 | 7 | 3 | 8 | 6 |

**Table 10.** Comparison of Algorithms and Final Ranking

| Algorithm | Best Total | Mean Total | Overall | Average Rank |
|---|---|---|---|---|
| **TRIDENT-DE** | 37 | 40 | 77 | 2.139 |
| **mLSHADE_RL** | 51 | 70 | 121 | 3.361 |
| **UDE3** | 63 | 65 | 128 | 3.556 |
| **CMA-ES** | 71 | 81 | 152 | 4.222 |
| **SaDE** | 85 | 86 | 171 | 4.750 |
| **EA4Eig** | 89 | 85 | 174 | 4.833 |
| **jDE** | 96 | 92 | 188 | 5.222 |
| **CLPSO** | 124 | 123 | 247 | 6.861 |

Table 7 reports best and mean performance under a common budget of $1.5 \cdot 10^5$ evaluations across synthetic and real-world problems. On the Lennard-Jones suite ($N$=10, 13, 38), TRIDENT-DE reaches energy minima on par with the strongest baselines while keeping the best-mean gap tight evidence that top results are reliably repeatable rather than isolated lucky runs. This contrasts with the pronounced variability seen in some competitors (e.g., large outliers for jDE on LJ-38), underscoring how the triple trial-vector ensemble, one-step greedy refinement, and micro-restarts absorb multi-modality without sacrificing diversity.

For the Tersoff-Si (B/C) potentials, the pattern remains favorable: TRIDENT-DE's best values are competitive or superior, and, crucially, the mean is often lower than that of many baselines, implying a higher probability of obtaining high-quality solutions in a typical run. The detailed rankings corroborate this view: by mean performance, TRIDENT-DE stays among the top ranks on physical potentials and several real-world tasks (e.g., TNEP, wireless coverage), highlighting robustness under constraints and irregular landscapes (see Tables 8 - 9).

Across real-world instances, behavior is category-dependent. In Transmission Network Expansion Planning and antenna placement/coverage, TRIDENT-DE shows excellent or strongly competitive outcomes with narrow best-mean spreads, indicating trustworthy single-run performance. In a few specialized settings, such as circular antenna design or the Cassini 2 trajectory problem, isolated top scores emerge from specific baselines (e.g., EA4Eig, CMA-ES), consistent with their aptitude for lower effective dimensional subspaces or smoother subregions. Still, when aggregating global evidence via mean-based rankings and win/placement totals, TRIDENT-DE achieves the best overall average rank among all contenders (Table 10), suggesting that its advantage is portable rather than instance-specific.

In the energy family, nuances appear. On DED variants, methods with strong adaptive dispersion (e.g., CMA-ES) often secure high placements, reflecting their ability to navigate plateau-like score profiles. Conversely, in ELD-1 without time coupling classical DE flavors may occasionally top the mean ranking, yet TRIDENT-DE remains consistently competitive and close to the optimal operating window, as evidenced by its mean figures in Table 7 and the per-problem ranks in Table 9. Practically, even when a "specialist" baseline dominates a narrow niche, TRIDENT-DE does not collapse in reliability, it maintains a small best-mean gap and stays near the top on average.

Overall, Table 7 reveals two complementary strengths: high best-case performance across a wide variety of instances and consistently strong mean performance that makes those peaks reproducible. When combined with the consolidated standings and Overall Average Rank in Tables 9- 10, the picture is clear: TRIDENT-DE delivers strong, stable, and widely transferable performance compared to the alternatives, with only a handful of exceptions where specific competitors exploit landscape idiosyncrasies to claim local wins.

## 4. Conclusions

The empirical evidence demonstrates that TRIDENT-DE delivers strong and transferable performance across heterogeneous settings from rugged physical landscapes (Lennard-Jones, Tersoff) to tightly constrained industrial/energy tasks (ELD/DED) and complex real-world applications (TNEP, wireless coverage, orbital design). Aggregated results in Table 7 show competitive best values accompanied by consistently tight best-mean gaps, indicating reproducible quality rather than isolated lucky hits. This picture is reinforced by the detailed standings in Table 9, where TRIDENT-DE maintains top-tier positions on physical potentials and several real-world tasks, while the final consolidated ranking in Table 10 yields the best Overall Average Rank among all contenders evidence of broad portability rather than niche specialization.

Mechanistically, the parameter-sensitivity study in subsection 3.3 indicates an intrinsically self-stabilising regime: the principal hyperparameters exert second-order effects across most domains, with targeted leverage for the stagnation threshold $\tau$ and the top-p fraction $\varphi$ (p-best) on heavily constrained landscapes. In Lennard–Jones and Tersoff, main-effect ranges remain small near the defaults, consistent with the triple operator ensemble, light jDE-style control on $F$, $C$ and one-step greedy line refinement acting as dampers against parameter oversensitivity. In energy scheduling (ELD/DED), strict feasibility and plateau-like regions elevate the roles of $\tau$ and $\varphi$ as control knobs for timely rejuvenation and exploitation-exploration balance, respectively. This behaviour is quantified in Tables 4, 5 and 6 and the accompanying figures.

Time-scaling evidence (Figure 5) adds a key dimension: wall-clock time grows approximately linearly with size in two representative domains ("GasCycle Thermal Cycle" and "Tandem Space Trajectory"), with no super-linear pathologies. The slightly higher curve of the latter reflects a domain-dependent additive evaluation cost rather than a shift in the algorithm's scaling rate, yielding predictability under load and a clean separation between stable algorithmic overhead and problem-dependent evaluation burden.

In sum, the findings articulate a triad of strengths: (i) consistently strong mean performance with small best-mean gaps (Table 7), (ii) dominant consolidated standings across diverse tasks (Tables 8-10), and (iii) favourable scaling without hidden overheads (Figure 5). The synergy among the triple trial-vector generator, line refinement, and adaptive micro-restarts distributes the burden of adaptation across exploration, exploitation, and diversity maintenance, explaining why hyperparameter effects remain modest over wide operating regions.

**Limitations.** Despite the positive aggregate view, certain boundaries are worth noting. In ELD/DED, performance is more sensitive to $\tau$ and $\varphi$ under constrained congestion, while defaults are safe operating points, local retuning can further stabilise progress (see subsection 3.3). In a few specialised scenarios (e.g., Cassini 2, circular antenna arrays), individual baselines attain isolated wins signalling landscape idiosyncrasies where added specialisation may help. Finally, the time-scaling study rests on two cases, although indicative, a broader scaling sweep (multiple sizes/dimensions/workloads) would strengthen external validity.

**Future Work.** Several promising avenues emerge. First, higher-level adaptivity (hyper-heuristics) could learn online operator-mix policies using credit assignment and success signals per generation, deepening the self-stabilising behaviour observed in 3.3. Second, targeted self-regulation of $\tau$ and $\varphi$ in constrained domains (ELD/DED) via bandit-style or Bayesian controllers may reduce plateau effects while preserving diversity. Third, integrating surrogate models for costly evaluations (e.g., lightweight GP/SVR) can leverage the observed linear scaling to maximise efficiency under tight budgets. Fourth, parallelisation (vectorised trials, GPU-friendly line refinement) promises additional wall-clock gains without altering stochastic dynamics. Fifth, extending to multi-objective and hard/soft constrained variants with explicit feasibility enforcement and adaptive penalties would probe robustness in more realistic settings. Finally, a theoretical strand (e.g., Markov-chain or drift analyses) could formalise the interplay among triple operators, restart, and refinement

that is empirically evident. These directions follow naturally from Table 7, Tables 8, 9 and 10, Figure 5, and subsection 3.3, aiming to convert empirical advantages into systematically scalable and theoretically grounded benefits.


1. Tapkin, A. (2023). A Comprehensive Overview of Gradient Descent and its Optimization Algorithms. International Advanced Research Journal in Science, Engineering and Technology, 10 (11), 37-45. https://doi.org/10.17148/IARJSET.2023.101106
2. Cawade, S., Kudtarkar, A., Sawant, S. & Wadekar, H. (2024). The Newton-Raphson Method: A Detailed Analysis. International Journal for Research in Applied Science & Engineering Technology (IJRASET), 12(11):729-734. https://doi.org/10.22214/ijraset.2024.65147
3. Bonate, P.L. (2001). A Brief Introduction to Monte Carlo Simulation. Clinical Pharmacokinetics 40(1):15-22. https://doi.org/10.2165/00003088-200140010-00002
4. Eglese, R. W. (1990). Simulated annealing: a tool for operational research. European journal of operational research, 46(3), 271-281.
5. Holland, J. H. (1975). Adaptation in natural and artificial systems. University of Michigan Press.
6. Deng, W., Shang, S., Cai, X., Zhao, H., Song, Y., & Xu, J. (2021). An improved differential evolution algorithm and its application in optimization problem. Soft Computing, 25, 5277-5298.
7. Pant, M., Zaheer, H., Garcia-Hernandez, L., & Abraham, A. (2020). Differential Evolution: A review of more than two decades of research. Engineering Applications of Artificial Intelligence, 90, 103479.
8. Charilogis, V., Tsoulos, I.G.,Tzallas, A., Karvounis, E. (2022). Modifications for the Differential Evolution Algorithm. Symmetry, 2022,14, 447. Doi: https://doi.org/10.3390/sym14030447
9. Charilogis, V., Tsoulos, I.G. A Parallel Implementation of the Differential Evolution Method. Analytics 2023, 2, 17–30.
10. Kennedy, J., & Eberhart, R. (1995). Particle swarm optimization. In Proceedings of ICNN'95 - International Conference on Neural Networks (Vol. 4, pp. 1942–1948). IEEE. Doi: https://doi.org/10.1109/ICNN.1995.488968
11. Charilogis, V., & Tsoulos, I. G. (2022). Toward an Ideal Particle Swarm Optimizer for Multidimensional Functions. Information, 13(5), 217. https://doi.org/10.3390/info13050217
12. Charilogis, V., Tsoulos, I.G. & Tzallas, A (2023). An Improved Parallel Particle Swarm Optimization. SN COMPUT. SCI. 4, 766. https://doi.org/10.1007/s42979-023-02227-9
13. Cao, Y., & Luan, J. (2024). A novel differential evolution algorithm with multi-population and elites regeneration. PLOS ONE, 19(4), e0302207. https://doi.org/10.1371/journal.pone.0302207
14. Sun, Y., Wu, Y., & Liu, Z. (2024). An improved differential evolution with adaptive population allocation and mutation selection. Expert Systems with Applications, 258, 125130. https://doi.org/10.1016/j.eswa.2024.125130
15. References Liang, J. J., Qin, A. K., Suganthan, P. N., & Baskar, S. (2006). Comprehensive learning particle swarm optimizer for global optimization of multimodal functions. IEEE Transactions on Evolutionary Computation, 10(3), 281–295.Doi: https://doi.org/10.1109/TEVC.2005.857610
16. References Hansen, N., & Ostermeier, A. (2001). Completely derandomized self-adaptation in evolution strategies. Evolutionary Computation, 9(2), 159–195. Doi: https://doi.org/10.1162/106365601750190398
17. Bujok, P., & Kolenovský, P. (2022). Eigen crossover in cooperative model of evolutionary algorithms applied to CEC 2022 single objective numerical optimisation. In 2022 IEEE Congress on Evolutionary Computation (CEC) (pp. 1–8). IEEE. https://doi.org/10.1109/CEC55065.2022.9870433
18. Dehghani, M., Trojovská, E., Trojovský, P., & Malik, O. P. (2023). OOBO: A new metaheuristic algorithm for solving optimization problems. Biomimetics, 8(6), 468. https://doi.org/10.3390/biomimetics8060468
19. Chauhan, D., Trivedi, A., & Shivani. (2024). A Multi-operator Ensemble LSHADE with Restart and Local Search Mechanisms for Single-objective Optimization. arXiv. https://doi.org/10.48550/arXiv.2409.15994
20. Nelder, J. A., & Mead, R. (1965). A simplex method for function minimization. The Computer Journal, 7(4), 308–313. Doi: https://doi.org/10.1093/comjnl/7.4.308
21. Dorigo, M., & Di Caro, G. (1999). Ant Colony Optimization. Proceedings of the 1999 Congress on Evolutionary Computation-CEC99* (Vol. 2, pp. 1470-1477). IEEE. https://doi.org/10.1109/CEC.1999.782657
22. Karaboga, D. (2005). An idea based on honey bee swarm for numerical optimization: Artificial bee colony (ABC) algorithm. Journal of Global Optimization, *39*(3), 459-471. https://doi.org/10.1007/s10898-007-9149-x
23. Tsoulos, I.G., Charilogis, V., Kyrou, G., Stavrou, V.N. & Tzallas,A. (2025). OPTIMUS: A Multidimensional Global Optimization Package. Journal of Open Source Software, 10(108), 7584. Doi: https://doi.org/10.21105/joss.07584.
24. Lee, Y., Filliben, J., Micheals,R. & Phillips ,J. (2012). Sensitivity Analysis for Biometric Systems: A Methodology Based on Orthogonal Experiment Designs. National Institute of Standards and Technology Gaithersburg (NISTIR), MD 20899. Doi: http://dx.doi.org/10.6028/NIST.IR.7855